PAPER

Check for updates

Fabrication of La^{3+} doped Ba$_{1-x}$La$_x$TiO$_3$ ceramics with improved dielectric and ferroelectric properties using a composite-hydroxide-mediated method†

U. Younas,[a] M. Atif, [iD] *[a] A. Anjum,[a] M. Nadeem,[b] T. Ali,[c] R. Shaheen,[c] W. Khalid[a] and Z. Ali[a]

Lanthanum (La^{3+}) doped Ba$_{1-x}$La$_x$TiO$_3$ ($x = 0.0$, 0.0025, 0.005, 0.0075) ceramics were synthesized by the composite-hydroxide-mediated method. Rietveld refinement of the XRD patterns confirmed the formation of a perovskite crystal structure that transforms from tetragonal to pseudo-cubic with La^{3+} doping content (x). Scanning electron microscopy displayed a dense and homogeneous microstructure with reduced grain size on La^{3+} doping. The frequency and temperature-dependent dielectric measurements showed an improvement in the dielectric permittivity, a decrease in the ferroelectric–paraelectric transition temperature, and an increase in the dielectric diffusivity with increasing La^{3+} doping content. Complex impedance analysis indicated the semiconducting behavior with a positive temperature coefficient of resistance effect, which could be explained in terms of a charge compensation mechanism in the donor doped BaTiO$_3$. The ferroelectric hysteresis loops revealed that these ceramics are ferroelectric in nature, while an improvement in the energy storage density and energy storage efficiency was observed for the doped samples due to reduced grain size on La^{3+} doping. Here, the sample with $x = 0.005$ has a high dielectric permittivity, a low dielectric tangent loss, and the highest energy storage efficiency. This makes this composition interesting for energy storage applications.

1. Introduction

Multilayer ceramic capacitors have seen tremendous development in recent years to meet the rising demands for miniaturization. Typically, multilayer ceramic capacitors are built up of individual dielectric layers that are 1 μm or thinner. To achieve this, it is necessary to employ ultrafine (nano- or submicron-sized) powders as raw materials, while also maintaining proper control over particle size and uniformity.[1,2] Lead-free ferroelectric ceramics have received much interest over the past few decades because of their non-toxic nature and exceptional electrical characteristics.[3] Among different lead-free ferroelectrics, barium titanate (BaTiO$_3$) is found to be a promising material for multilayer ceramic capacitors because of its exceptional dielectric characteristics, including a high dielectric constant ($>10^3$) and reduced dielectric loss.[4] However, these characteristics can only be achieved within a small temperature range close to the ferroelectric phase transition. Therefore, to

resolve this shortcoming, doping with a suitable element at Ba-, Ti-, or both sites has been frequently used to fabricate BaTiO$_3$-based materials for more viable multilayer ceramic capacitors.[5,6]

Trivalent rare-earth (RE^{3+}) ions are typically utilized to tune the electrical characteristics of ferroelectric perovskite BaTiO$_3$ ceramics because of their intermediate size and charge relative to Ba^{2+} and Ti^{4+} ions.[7] In general, depending on ionic size, small-sized RE^{3+} ions (like Yb^{3+}) dope only on the Ti-site with charge compensation by oxygen vacancies, intermediate-sized RE^{3+} ions (such as Gd^{3+}, Er^{3+}) may dope equally on each Ba- and Ti-sites, and large-sized RE^{3+} ions (such as La^{3+}, Pr^{3+}) dope exclusively on the Ba-site.[8] However, among different doping mechanisms, the Ba-site doping of RE^{3+} ions is a subject of discussion for a long time, as the dc resistivity of ceramics at ambient temperature can exhibit either semiconducting and/or insulating behavior, depending on the dopant concentration and/or processing parameters.[9–12] Since, the pure BaTiO$_3$ is a good insulator with a resistive value of $\sim10^{10}$ Ωcm at room temperature and a large energy gap $E_g = 3.5$ eV. When BaTiO$_3$ is doped with extremely low concentrations (<0.5 at%) of higher valence foreign ions as La^{3+}, Gd^{3+}, Dy^{3+} on the Ba-site, it usually exhibits semiconducting behavior, implying compensation *via* an electronic mechanism.[13,14] However, for higher dopant contents (>1 at%), the compensation occurs through an ionic

[a]Functional Materials Lab, Department of Physics, Air University, PAF Complex E-9, Islamabad, Pakistan. E-mail: matif@mail.au.edu.pk

[b]Polymer Composite Group, Directorate of Science, PINSTECH, Islamabad, Pakistan

[c]Physics Division, Directorate of Science, PINSTECH, Islamabad, Pakistan

† Electronic supplementary information (ESI) available. See DOI: https://doi.org/10.1039/d2ra06640h

mechanism resulting in the formation of cation vacancies and insulating behavior.[9,15] Among different trivalent rare-earth ions, lanthanum (La^{3+}) is found to be one of the most investigated RE^{3+} dopant which behaves as a donor dopant and usually replaces Ba^{2+} ions in the crystal lattice of $BaTiO_3$ at smaller amount of La^{3+} doping content (<1 at%), because La^{3+} ions are too large to replace Ti^{4+} ions on the Ti-site. Moreover, La^{3+} ions have a different valence than Ba^{2+}, causing a charge imbalance that produces n-type semiconductivity. Thus, the charge compensation involves the formation of electrons, electron holes, or titanium (V_{Ti}) and oxygen (V_O) vacancies in the ceramic materials, resulting in a variation of their electrical characteristics.[16] Morrison et al. reported the semiconducting character in La^{3+} doped $BaTiO_3$ ceramics, which is attributed to the loss of oxygen during sintering at high temperatures (≥ 1350 °C) in air.[17] Ganguly et al. obtained a compositional induced phase transition from tetragonal to cubic symmetry with the increase in La^{3+} doping content in $BaTiO_3$ ceramics.[18] They also found an increase in the dielectric permittivity along with the broadening of dielectric peak. Wang et al. showed that increasing the La^{3+} doping content in $BaTiO_3$ ceramics inhibits the grain growth and that both the room and maximum dielectric constants diminish monotonously.[19] Puli et al. explored the effect of La^{3+} doping on the dielectric and ferroelectric properties of $Ba_{1-x}La_xTiO_3$ ($x = 0.0$–0.003) semiconducting ceramics.[20] The dielectric constant and recoverable energy storage density are found to be improved by La^{3+} doping. However, due to high hysteresis loss, a small decrease of 12% in the energy storage efficiency is obtained for the doped samples. Moreover, for both undoped and doped samples, room temperature semiconducting behavior is observed with positive temperature coefficient of resistivity (PTCR) behavior at Curie temperature (T_c) due to the electron compensation mechanism. Recently, Kumar et al. reported a significant enhancement in the dielectric and energy storage properties of La^{3+} doped $Ba_{1-z}La_z Ti_{0.95}Sn_{0.05}O_3$ ($z = 0.0$–0.035) ceramics.[21] The highest value of energy storage efficiency (63%) for a $z = 0.035$ sample is found to be 8.4 times higher than that of an undoped sample. According to them, the observed improvement in the dielectric constant and energy storage density along with a reduction in hysteresis loss is attributed to reduced grain size due to La^{3+} doping. Hence, in light of the aforementioned studies, it follows that the effects of dopant concentration and grain size may be optimized in order to modify the dielectric and energy storage characteristics of $BaTiO_3$ ceramics.

During the past decade, with the requirement of size reduction in electronic devices, a lot of research work has been put in the processing of nanomaterials of different shapes and sizes with the aim of enhancing their electronic, optical, and structural properties. The conventional approach for fabricating $BaTiO_3$ ceramics is a solid-state reaction followed by a ball milling and high-temperature sintering process.[22] However, in recent years, different low-temperature chemical routes have been developed, including the hydrothermal,[23] sol–gel,[24] solvothermal,[25] and microwave processing technique.[26] For all of these chemical routes, various synthesis parameters (like reaction temperature and time, sintering temperature,

pressure, surfactant, etc.) are required to optimize and control for synthesizing nanostructured $BaTiO_3$ ceramics. However, the composite-hydroxide-mediated (CHM) method is found to be an environmentally friendly, cost-effective, fast, mass-productive, and one-step process to produce a wide range of nanostructures. The $BaTiO_3$ nanostructures have been prepared using the CHM method, wherein the influence of different reaction times and temperatures on the morphological structures of prepared particles has been explored.[27,28] It is found that the particle size, surface smoothness, and crystal structure of these CHM-prepared nanostructures strongly depend on the processing conditions. Xie et al. also reported the synthesis of fine-grained tetragonal $BaTiO_3$ nanoparticles by the CHM method.[29] The obtained powder was then compacted and sintered at relatively lower temperature of 1200 °C for 4 h, which presented a high value of dielectric constant due to much higher density ($\sim$99%) than that of commercially available $BaTiO_3$ powder. To the best of our knowledge, very limited work has been found on the dielectric properties of $BaTiO_3$ ceramics prepared by the CHM method. Furthermore, no attempt has been made to prepare doped $BaTiO_3$ ceramics using the CHM method, as well as to investigate the ferroelectric and energy storage properties of the CHM prepared $BaTiO_3$ ceramics. Therefore, in this work, we prepared different compositions of La^{3+} doped $Ba_{1-x}La_xTiO_3$ ceramics ($x = 0.0$, 0.0025, 0.005, 0.0075) using a composite-hydroxide-mediated method under optimum conditions. The influence of La^{3+} doping on the microstructure, dielectric, ferroelectric, and energy storage properties, along with the sintering of resulting powders to produce dense, La^{3+} doped $Ba_{1-x}La_xTiO_3$ ceramics was investigated. Moreover, the La^{3+} doped prepared ceramics are also explored in terms of their semiconducting properties with a PTCR effect.

2. Experimental

La^{3+} doped $Ba_{1-x}La_xTiO_3$ ($x = 0.0$, 0.0025, 0.005, 0.0075) ceramics were prepared using the composite-hydroxide-mediated (CHM) method. A mixture of 20 g of mixed hydroxides (NaOH/KOH = 51.5 : 48.5) was put into a 50 ml Teflon vessel. Afterward, a mixture of barium nitrate [$Ba(NO_3)_2$, Sigma-Aldrich, $\geq$99%], lanthanum nitrate [$La(NO_3)_2 \cdot 6H_2O$, Sigma-Aldrich, $\geq$99%], and titanium oxide [TiO_2, Sigma-Aldrich, $\geq$99%] at 10 mmol each was added to the vessel as per their stoichiometric ratio. The vessel was then put in a heating oven at 200 °C for 72 h. After the chemical reaction, the vessel was taken out of the oven and cooled down to room temperature. To eliminate hydroxides on the surface of the particles, the product was filtered and washed many times with deionized water. Finally, the obtained powders were dried overnight at 100 °C in an oven and annealed in the furnace at 700 °C for 3 h under ambient conditions. The calcined powders were mixed with 5 wt% binder (polyvinyl alcohol) and then uniaxially pressed by applying a compaction pressure of 5 ton per cm^2. The pelletized samples were then sintered at 1200 °C for 4 h in a conventional furnace with a heating/cooling rate of 5 °C min^{-1}.

The structural characterization of the prepared $Ba_{1-x}La_xTiO_3$ samples was examined with an X-ray diffractometer (ARL EQUINOX 3000). Rietveld refinement was carried out with the help of Fullprof software for a more precise analysis. The surface morphology of the prepared samples was studied using a field-emission scanning electron microscope (FESEM, TESCAN MAIA3). Before electrical measurements, both sides of the sintered pellets were polished and coated with silver paste. Afterwards, the silver-coated pellets were dried at 100 °C for 2 h in a heating oven. Impedance spectroscopy was carried out using an Impedance analyzer (Agilent 4294A, USA) at different temperatures (303–463 K) within the frequency range of 40–10^7 Hz. The room temperature ferroelectric measurements were performed by a Precision Multiferroic II ferroelectric tester (Radiant Technology Inc., USA).

3. Results and discussion

3.1. XRD analysis

Fig. 1(a–d) shows the X-ray diffraction (XRD) patterns of La^{3+} doped $Ba_{1-x}La_xTiO_3$ ($x = 0.0, 0.0025, 0.005, 0.0075$) samples sintered at 1200 °C for 4 h. The XRD peaks for the pure $BaTiO_3$ sample (*i.e.*, $x = 0.0$) belong to a tetragonal perovskite phase in accordance with the JCPDS file no. 05-0626.[30] As seen from Fig. 1(a), no un-indexed peak is observed in the XRD pattern of a pure sample, which indicates the formation of a pure single-phase sample. Here, the splitting of (002)/(200) and (112)/(211) diffraction peaks at $2\theta = 45°$ and $56°$, respectively, confirmed the presence of tetragonal phase for the pure sample. With the doping of La^{3+} ions in place of Ba^{2+} in $BaTiO_3$ lattice, we found that all peaks correspond to tetragonal phase and the XRD peaks shift towards the higher 2θ values with increasing La^{3+} doping content (x). This behavior of peak shifting is attributed to the difference between the ionic radii of dopant ($La^{3+} = 1.16$ Å) and host ($Ba^{2+} = 1.42$ Å) ions. To estimate the structural parameters, Rietveld refinement on the XRD patterns of pure $BaTiO_3$ and La^{3+} doped $Ba_{1-x}La_xTiO_3$ samples was employed using the Fullprof program. The figure demonstrates that the calculated XRD patterns provide the best match to the experimental data, with a goodness-of-fit value ($\chi^2 = 1.08–1.62$) that is close to the value obtained from the experiment. The estimated values of lattice constants (a, c), cell volume (V), and goodness of fit (χ^2) are presented in Table 1. We observed that as La^{3+} doping content (x) increases, the value of lattice constant a increases while the values of c and V decrease slightly due to the smaller ionic radii of La^{3+} compared to Ba^{2+} ions. Further,
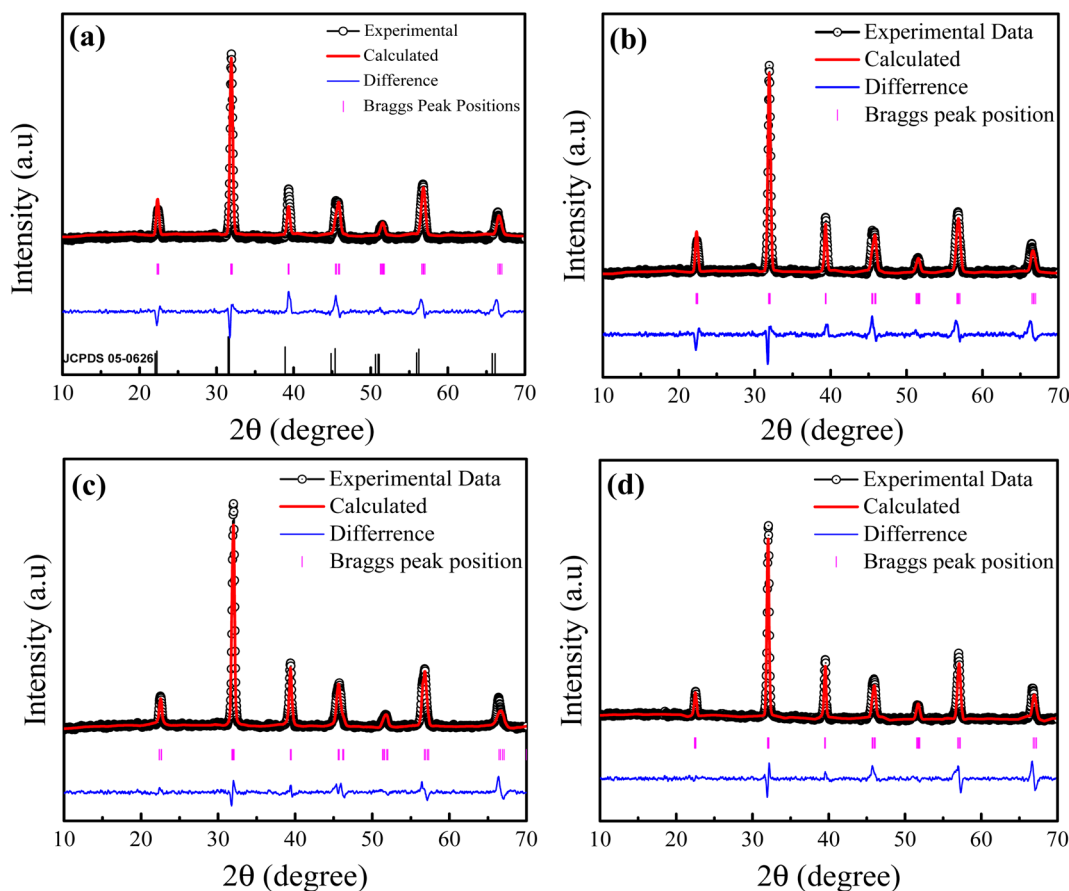

Fig. 1 Rietveld refinement of the XRD data of La^{3+} doped $Ba_{1-x}La_xTiO_3$ ceramics with (a) $x = 0.0$, (b) $x = 0.0025$, (c) $x = 0.005$, and (d) $x = 0.0075$. Here, the experimental data are depicted by the black circle, the estimated intensities by the red line, the difference between both intensities by the blue baseline, and the allowed Bragg's position by the magenta vertical lines.

Table 1 Compositional variation of lattice constant (a, c), tetragonality ratio (c/a), cell volume (V), goodness of fit (χ^2), average grain size (D), sintered density (ρ_s), relative density (ρ), Curie temperature (T_c), and degree of diffuseness (γ) for the La^{3+} doped Ba$_{1-x}$La$_x$TiO$_3$ ceramics

Sample (x)	a (Å)	c (Å)	c/a	V (Å^3)	χ^2	D (μm)	ρ_s (g cm^{-3})	ρ (%)	T_c (K)	γ
0.00	3.967	3.998	1.0078	62.92	1.08	3.06	5.77	96	409	1.18
0.0025	3.968	3.994	1.0065	62.90	1.10	1.10	5.60	93	405	1.26
0.005	3.971	3.982	1.0027	62.76	1.82	0.98	5.66	94	398	1.33
0.0075	3.972	3.978	1.0015	62.75	1.43	0.89	5.54	92	393	1.49

with increasing La^{3+} doping content, it can be seen that the value of tetragonality ratio (c/a) approaches to 1 suggesting a probable change in the unit cell symmetry from tetragonal to pseudo-cubic structural phase.[31]

Since, the ionic radius of La^{3+} ions lies between the respective ionic radii of Ba^{2+} and Ti^{4+} ions.[32] Thus, to find out the probability of whether La^{3+} ions occupy the Ba-site or Ti-site in the BaTiO$_3$ lattice, we used the Goldschmidt tolerance factor (t) which indicates the stability and distortion in the perovskite structure (ABO$_3$) and is given by:[33]

$$t = \frac{r_A + r_o}{\sqrt{2}\,(r_B + r_o)} \tag{1}$$

where r_A, r_B, and r_o are the ionic radii of A cation (Ba^{2+}), B cation (Ti^{4+}), and oxygen anion (O^{2-}). Generally, the value of the tolerance factor for a stable perovskite structure is between 0.88 and 1.06.[34] Here, we have calculated the tolerance factor of La^{3+} ions to occupy completely Ba- and Ti-sites, and the obtained values are found to be 0.995 and 0.871 for the Ba- and Ti-sites, respectively. Since the value of the tolerance factor to occupy Ti-site is less than 0.88, which excludes the possibility of La^{3+} replacing the Ti^{4+} ions at Ti-site. Hence, La^{3+} ions have a greater probability of replacing Ba^{2+} ions at the Ba-site.

3.2. SEM analysis

Fig. 2(a–d) displays the field-emission scanning electron microscopy (FE-SEM) images of the prepared Ba$_{1-x}$La$_x$TiO$_3$ (x = 0.0, 0.0025, 0.005, 0.0075) samples. All of these images were taken from the fractured surfaces of pelletized samples. As seen
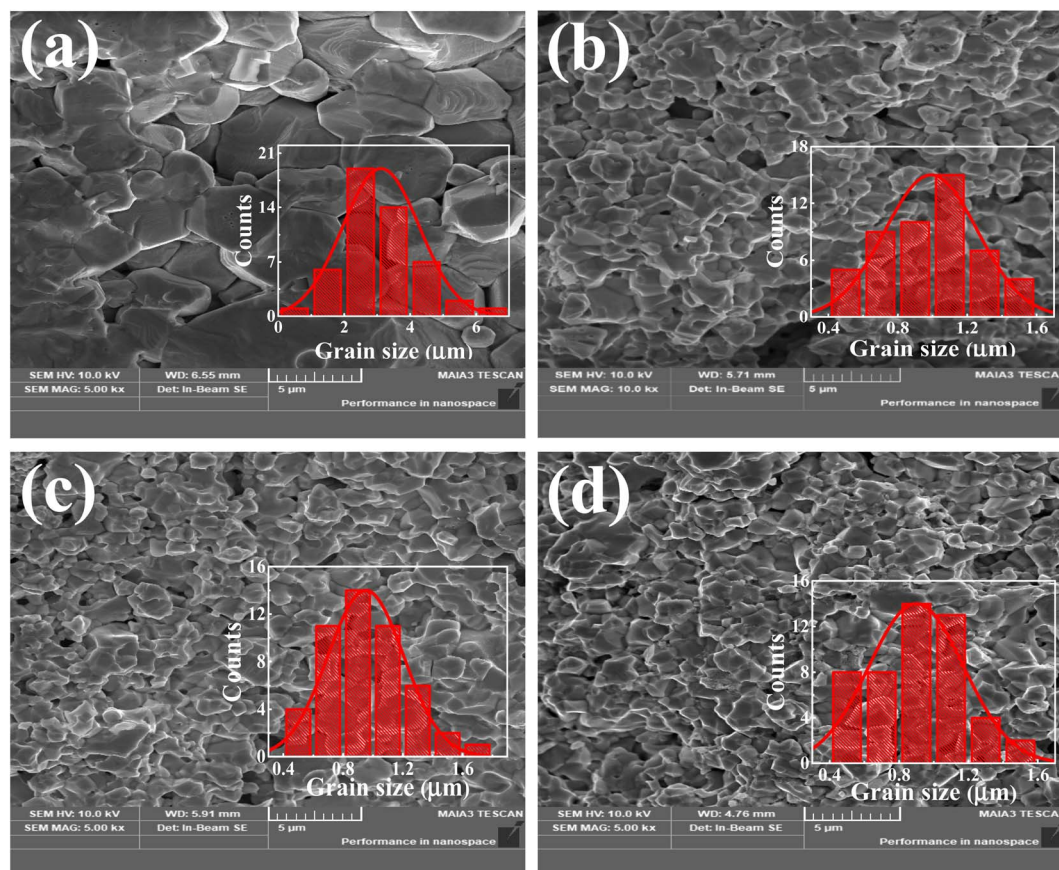

Fig. 2 SEM micrographs of La^{3+} doped Ba$_{1-x}$La$_x$TiO$_3$ ceramics with (a) x = 0.0, (b) x = 0.0025, (c) x = 0.005, and (d) x = 0.0075. Insets of (a–d) show the grain size distribution.

from Fig. 2(a), the pure BaTiO$_3$ sample (*i.e.*, $x = 0.0$) shows a dense microstructure consisting of bigger grains wherein a few smaller grains and grains with terraced surfaces are also visible among them. Here, the presence of discontinuous grain growth and terraced surfaces could be attributed to the enhanced mass transport phenomenon due to formation of oxygen vacancies at higher sintering temperatures.[21] Therefore, to estimate the average grain size (D) in a pure sample, the grain size distribution was estimated from the SEM image using ImageJ software and found to be ~3 μm (see inset of Fig. 2(a)). With the addition of La^{3+} ions, there is a considerable reduction in grain sizes along with uniform and denser microstructures for the La^{3+} doped Ba$_{1-x}$La$_x$TiO$_3$ samples, as shown in Fig. 2(b–d). Further, the insets of Fig. 2(b–d) show the distribution of grain size in the doped samples, and the estimated average grain sizes (D) are presented in Table 1. Here, it is observed that the average grain size of the $x = 0.005$ sample is reduced by ~70% as compared with the pure sample. This apparent decline in grain size due to La^{3+} doping is attributed to an overall decrease in the diffusion rate during the sintering process which might suppress the formation of oxygen vacancies. Similar variation in the grain sizes have been reported for small values of La^{3+} doping in BaTiO$_3$ and Pb(Zr$_{1-x}$Ti$_x$)O$_3$.[18,35] Moreover, the relative density (ρ) was estimated using the theoretical density of BaTiO$_3$ ($\rho_{th} = 6.02$ g cm^{-3}) and the sintered density

(ρ_s) of the pelletized samples calculated by the Archimedes method. The values of ρ for the prepared samples are ≥92% (see Table 1), which indicates better densification in the microstructures of sintered samples prepared by the CHM method. These values also showed that pure BaTiO$_3$ had a higher density than La^{3+}-doped samples. The observed decrease in the value of ρ with La^{3+} doping content is attributed to the fact that, when La^{3+} occupies the Ba-site as a donor, cation vacancies and radius discrepancies between La^{3+} and Ba^{2+} deform the lattice. This could hinder densification by making mass mobility more difficult in compact structures.[19,26]

3.3. Dielectric properties

Fig. 3(a–d) shows the temperature-dependent behavior of real part of dielectric permittivity (ε') and dielectric tangent loss (tan δ) for the La^{3+} doped Ba$_{1-x}$La$_x$TiO$_3$ ($x = 0.0, 0.0025, 0.005, 0.0075$) samples measured at different frequencies (1 kHz to 1 MHz) between the temperature range of 303 K to 463 K. It can be seen that, for the pure BaTiO$_3$ sample ($x = 0.0$), the ε' value begins to increase gradually with increasing temperature and reaches a maximum value at 409 K and then decreases smoothly with further increase in temperature (Fig. 3(a)). Here, the increasing trend of ε' with temperature is accredited to the orientational polarization which is associated with the thermal motion of dipoles. The specific temperature at which ε' has
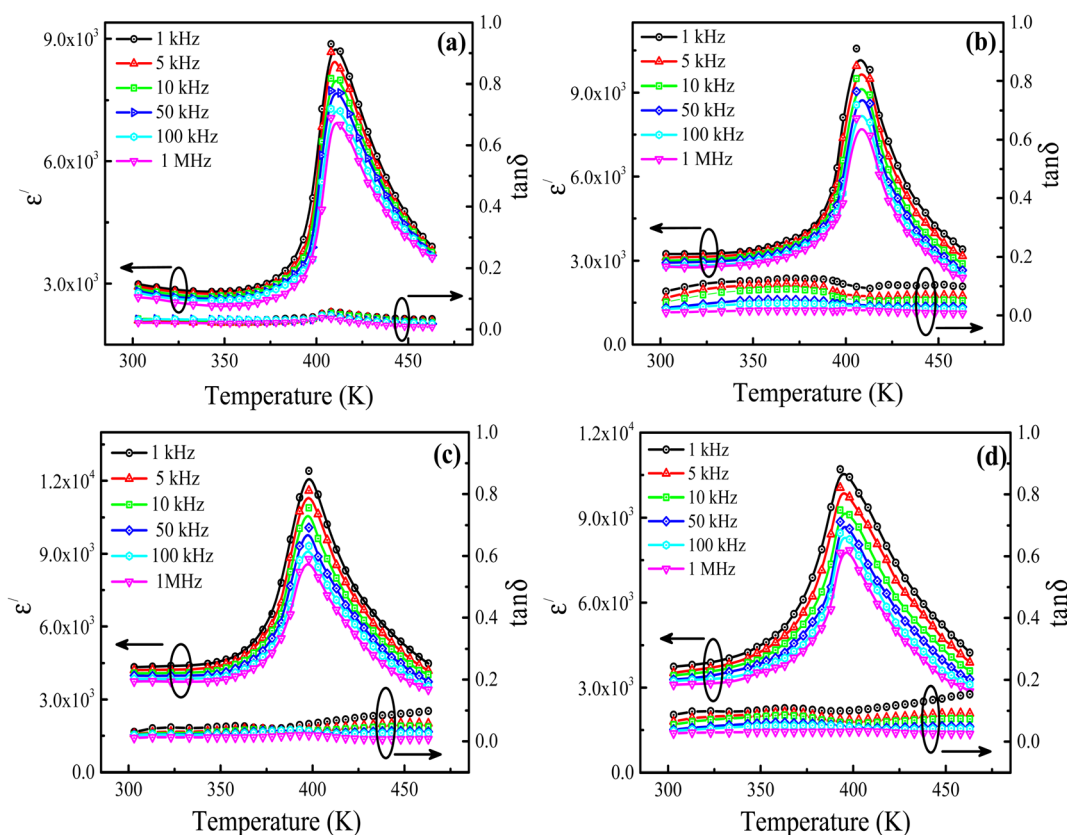

Fig. 3 Temperature-dependent behavior of the real part of dielectric permittivity (ε') and dielectric tangent loss (tan δ) for the La^{3+} doped Ba$_{1-x}$La$_x$TiO$_3$ ceramics (a) $x = 0.0$, (b) $x = 0.0025$, (c) $x = 0.005$, and (d) $x = 0.0075$ measured at different frequencies (1 kHz to 1 MHz) between the temperature range of 303 K to 463 K.

a maximum value is defined as the Curie temperature (T_c). At this temperature, the ferroelectric phase transforms into the paraelectric phase, followed by a structural transition from tetragonal symmetry to cubic. A similar transition temperature was also found in the literature for $BaTiO_3$.[19,21] However, a small difference in the values of ε' and T_c might be caused by the grain size effect. Further, the Curie temperature (T_c) of a pure sample is observed to continually decrease from 409 K to 393 K with increasing La^{3+} doping content (x) in $Ba_{1-x}La_xTiO_3$ (see Table 1). While, the value of ε' is found to increase by La^{3+} doping at the Ba^{2+} site, when compared with a pure sample. Here, the observed trend of T_c and ε' with La^{3+} doping might be associated with the reduction in grain size and smaller ionic dopant. Also, the replacement of Ba^{2+} by the higher valence La^{3+} ions generates cation vacancies on the Ti^{4+} site to maintain charge neutrality, which in turn introduces distortion in the TiO_6 octahedra.[21,36] Thus, these distorted TiO_6 octahedra break the long-range ordering and assist in the reorientation of ferroelectric domains, which results in the improved ε' value of $BaTiO_3$ with La^{3+} doping. Here, the observed ε' value at room temperature for the pure $BaTiO_3$ and La^{3+} doped $BaTiO_3$ samples is relatively higher than the values reported for similar systems,[13,19,26,34] which might be related to the grain size effect. It is well known that the maximum value of ε' in the $BaTiO_3$ ceramics is obtained at a grain size of 1.0 μm as a result of the

optimum density and mobility of 90° domain walls in the prepared sample.[37] Since the average grain size of prepared $BaTiO_3$ and La^{3+} doped $BaTiO_3$ samples are 3 μm (>1.0 μm) and 0.89–1.1 μm (~1.0 μm), respectively (see Fig. 2). Thus, the La^{3+} doped $BaTiO_3$ samples exhibit higher values of ε' in comparison to pure $BaTiO_3$ sample. However, among the doped samples, the sample with $x = 0.005$ sample provides the highest value of ε' due to the dominant effect of fine grains (0.98 μm) with uniform distribution and enhanced charge carrier concentration. Moreover, the figure reveals that the ε' value decreases slightly with increasing frequency over the entire temperature range, and the ε' peak is found to be temperature independent for all prepared samples. While, a visible broadening of the dielectric peaks can be seen, suggesting that the observed phase transition is of the diffuse-type. Typically, such broadening of the dielectric peak results from compositional fluctuation, merging of micro to macro polar regions, and/or doping induced disorder in the crystal lattice.[38] Moreover, the low values of dielectric tangent loss ($\tan \delta$) between 0.036 and 0.55 are observed in the prepared $Ba_{1-x}La_xTiO_3$ samples, and the values of $\tan \delta$ are found to slightly increase with La^{3+} doping compared to pure $BaTiO_3$ sample (see Fig. 2(a–d)). However, above the Curie temperature, there is an abrupt increase in $\tan \delta$ value with increasing temperature, which would be the direct consequence of higher electrical conductivity.[21]
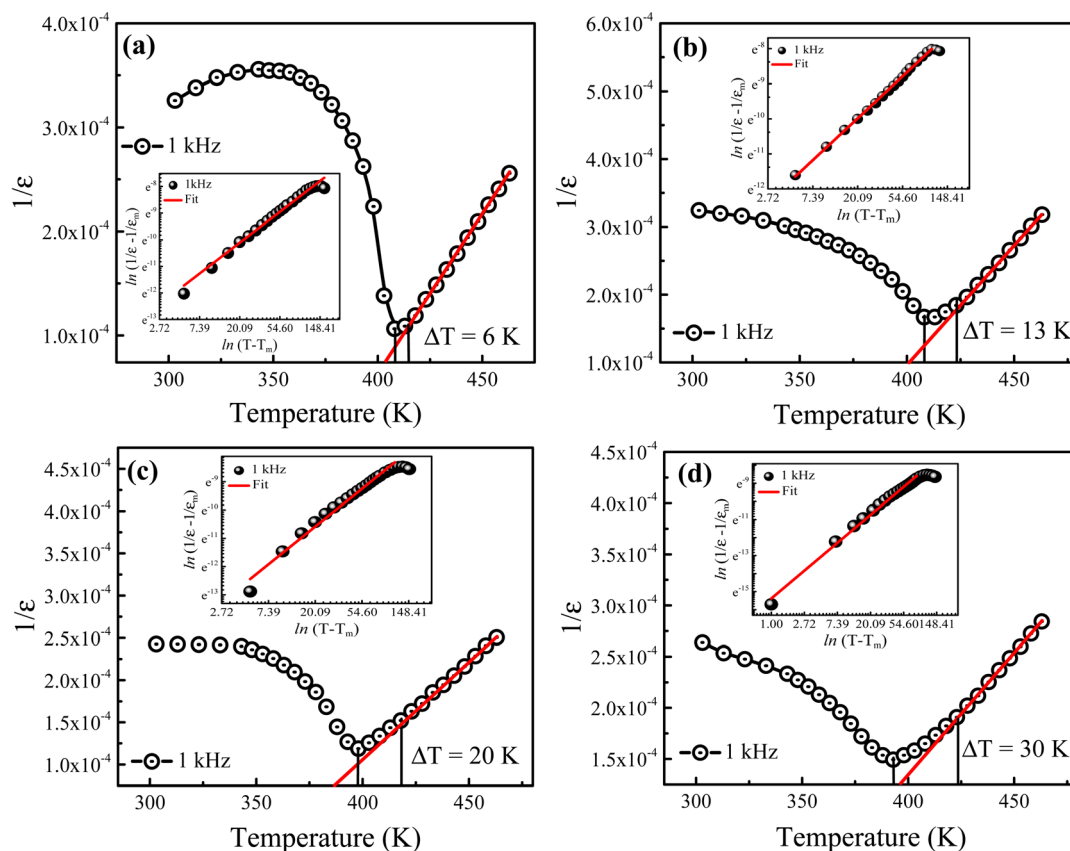

Fig. 4 Temperature dependence of the inverse of dielectric permittivity (ε') for the La^{3+} doped $Ba_{1-x}La_xTiO_3$ ceramics with (a) $x = 0.0$, (b) $x = 0.0025$, (c) $x = 0.005$, and (d) $x = 0.0075$ measured at a representative frequency of 1 kHz. Insets of (a–d) display the graphs of $\ln(1/\varepsilon_r - 1/\varepsilon_m)$ versus $\ln(T - T_m)$ for the prepared samples.

To further investigate the dielectric dispersion and diffusiveness for the prepared $Ba_{1-x}La_xTiO_3$ samples, the temperature dependence of the inverse of ε' is plotted for the prepared samples at a particular frequency of 1 kHz as presented in Fig. 4(a–d). As seen in the figure, all samples exhibit a deviation from the Curie–Weiss law because of a small discrepancy among the maximum ε' temperature (T) and the temperature at which ε' starts to depart from the Curie–Weiss law (T_m). To describe this deviation, a modified version of the Curie–Weiss law might be used:[39]

$$\frac{1}{\varepsilon_r} - \frac{1}{\varepsilon_m} = \frac{(T - T_m)^{\gamma}}{C} \qquad (2)$$

where ε_r is the dielectric permittivity at T, ε_m is the dielectric permittivity at T_m, C is the constant, and γ is the degree of diffuseness whose value may vary from 1 (normal ferroelectric) to 2 (relaxor ferroelectric). Insets of Fig. 4(a–d) display the graphs of $\ln(1/\varepsilon_r - 1/\varepsilon_m)$ as a function of $\ln(T - T_m)$ for the prepared samples at 1 kHz. It is obvious that these graphs display a linear relationship and by fitting with eqn (2), the values of diffuseness degree (γ) are obtained from the slopes of these graphs, which are presented in Table 1. Here, the value of $\gamma = 1.18$ for the pure $BaTiO_3$ sample ($x = 0.0$) reveals the normal ferroelectric behavior while the value of γ gradually increases from 1.18 to 1.49 with increasing La^{3+} doping in $BaTiO_3$, which

indicates that the diffuseness in the phase transition increases with La^{3+} doping. Here, the observed increase in the diffuseness is due to cation disordering effect and the difference between the ionic radii of dopant and host ions. This phenomenon plays an important role in increasing the compositional fluctuation, which leads to diffused phase transition.[40,41]

3.4. Impedance analysis

Impedance spectroscopy (IS) is a technique that may be utilized to investigate the electrical homogeneity within ceramic materials. It is well known that ceramic materials have an electrically heterogeneous structure, consisting of semiconducting grains (Gs) that are isolated by an insulating grain boundary (GBs), particularly when doping is included. Consequently, impedance analysis was used to analyze and extract the contributions of the Gs and GBs resistance from the material's overall resistance.[42] Fig. 5(a–d) depicts the complex impedance plane plots (Z' *vs.* Z'') of $Ba_{1-x}La_xTiO_3$ ($x = 0.0, 0.0025, 0.005, 0.0075$) samples measured at various temperatures. As seen in the figure, pure $BaTiO_3$ and La^{3+} doped $BaTiO_3$ samples exhibit two overlapping semicircular arcs at each temperature. Here, the appearance of two semicircular arcs indicates distinct electroactive regions resulting from the presence of Gs and GBs with different relaxation times.[42] Typically, the conductive bulk region exhibits
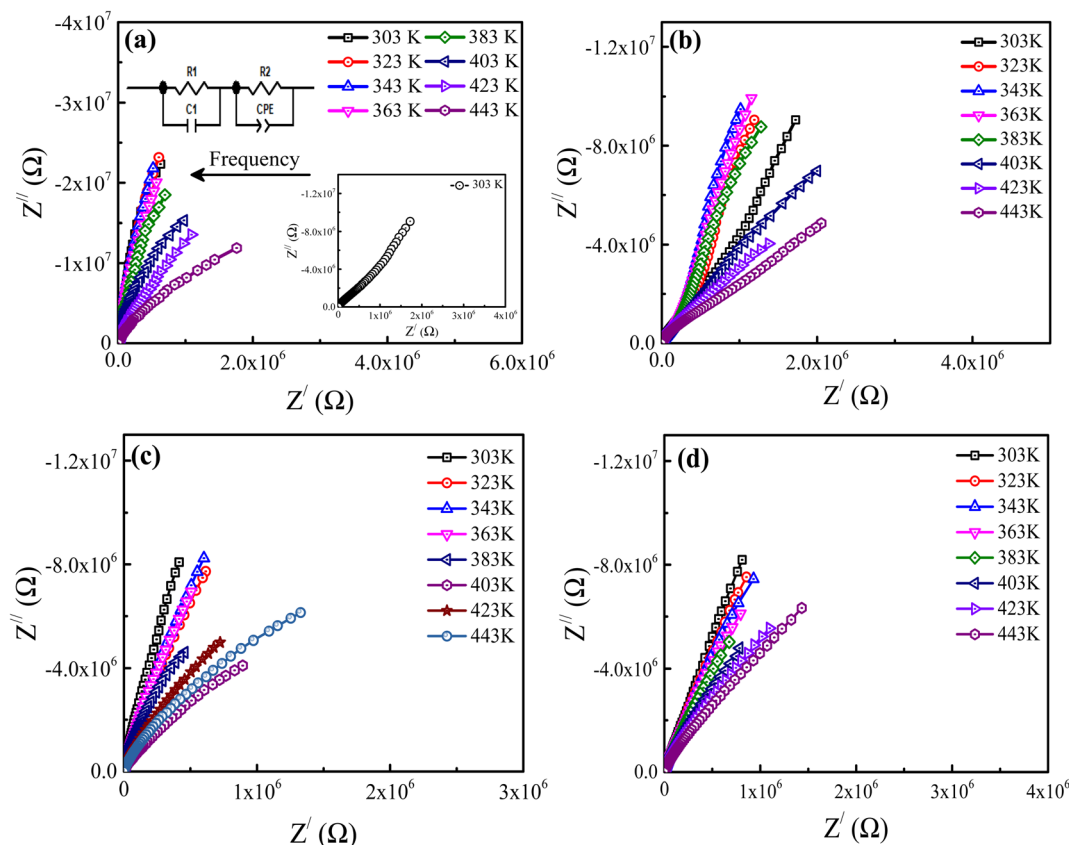

Fig. 5 Complex impedance plane plots (Z' *vs.* Z'') of $Ba_{1-x}La_xTiO_3$ ceramics with (a) $x = 0.0$, (b) $x = 0.0025$, (c) $x = 0.005$, and (d) $x = 0.0075$ measured at various temperatures. Insets of (a) show the enlarged Insets of (a) show the impedance plane plot measured at 303 K and the equivalent circuit model. Here, the arrow shows the direction of the applied frequency.

relaxation at higher frequencies; hence, the semicircular arc's reduced diameter that forms on the higher frequency region and passes through the origin, is termed as the electroactive region's Gs. Similarly, the GBs relate to the region defined by the semicircular arc's large diameter at lower frequencies and a more resistive electroactive region. In general, the x-intercept of these semicircular arcs gives the expected values of sample resistance for GBs and Gs. It can be observed in the figure, both the size and shape of the semicircular arcs vary with the increase in temperature and La^{3+} doping concentration in the prepared ceramics, showing an overall changes in the resistive characteristics. Thus, to estimate the expected variations in the resistance and to assign distinct electroactive regions, we have used the ZView software to fit an equivalent circuit model of $(R_1 - C_1)(R_2 - CPE)$ to our experimental data. Here, the resistance R, capacitance C, and constant phase element CPE are the components of this circuit. CPE is typically a deviation from the real capacitance behavior, suggesting the presence of dissimilar relaxations that have a similar relaxation time. Usually, the following expression is used to compute the capacitance of CPE:[43]

$$C = (CPE)^{\frac{1}{n}} R^{\left(\frac{1-n}{n}\right)} \tag{3}$$

where n represents the dispersion parameter and takes on the value 1 for an ideal capacitor and the value 0 for an ideal resistor. On the basis of the fitting parameters given in the ESI (Table S1†) for each temperature and La^{3+} doping content (x), the capacitance values (C_1) derived from the first circuit are comparable to the geometric values for Gs (10^{-11} to 10^{-13} Fcm^{-1}).[44] However, the capacitance values (C_2) derived from the second circuit are equivalent to the geometric value for GBs (10^{-8} to 10^{-10} Fcm^{-1}).[44] Here, the C_2 values for all samples at each temperature were calculated using eqn (3). Thus, we determined that GBs and Gs conduction are responsible for the semicircular arcs seen at lower and higher frequencies, respectively. Usually, the resistance of GBs (R_{GBs}) is found to be much higher than the Gs resistance (R_{Gs}). However, compared to an undoped sample, no significant variation of the R_{Gs} is observed while a significant decrease in the value of R_{GBs} is observed with a small doping of La^{3+} in $BaTiO_3$. As seen from Table S1,† the values of R_{Gs} and R_{GBs} initially decrease up to $x = 0.005$ and then slowly increase for $x = 0.0075$ sample. Here, the smallest value of resistance obtained for the $x = 0.005$ sample is probably attributed to more uniform incorporation of dopant in the $BaTiO_3$ lattice and a high concentration of free charge carriers, which will be discussed in detail in the next paragraph.
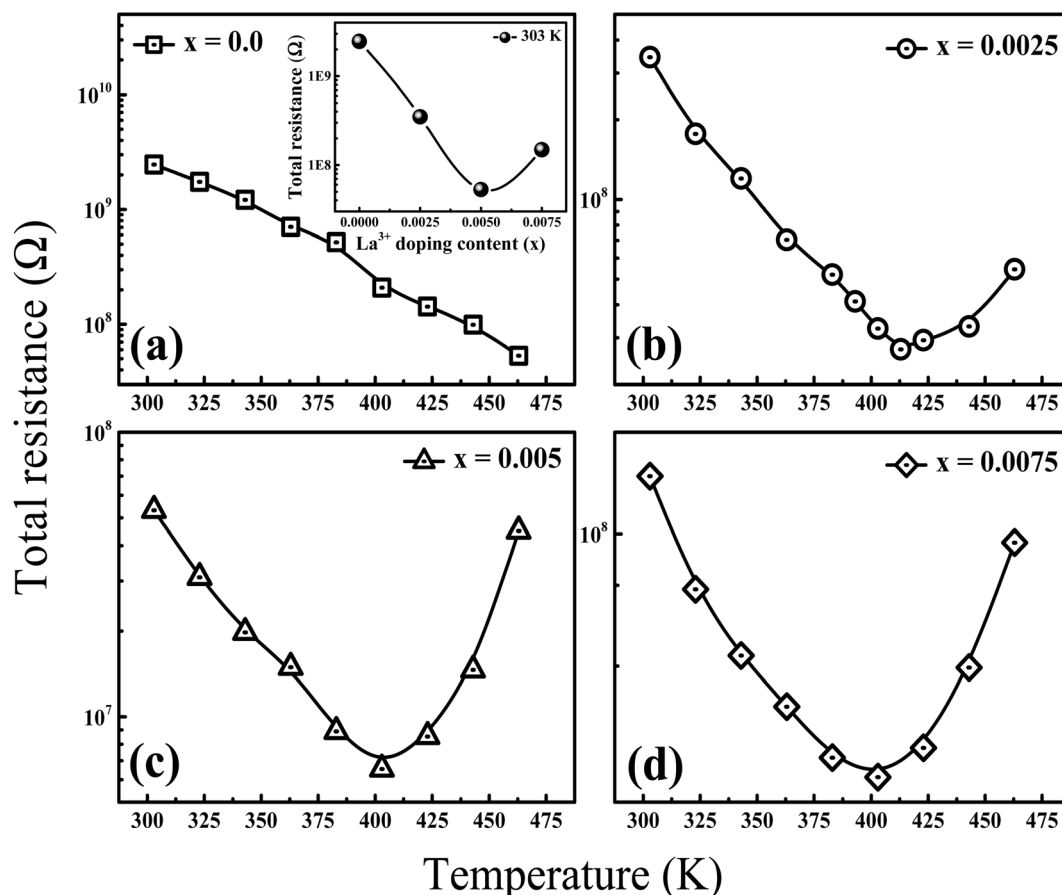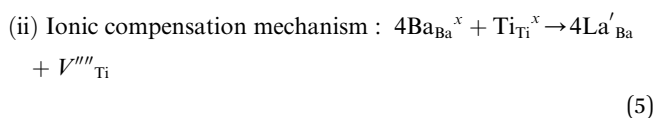

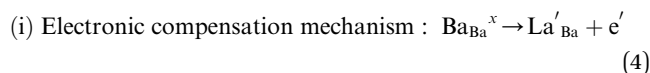**Fig. 6** Temperature dependence of the total resistance (R_T) in the prepared $Ba_{1-x}La_xTiO_3$ ceramics with (a) $x = 0.0$, (b) $x = 0.0025$, (c) $x = 0.005$, and (d) $x = 0.0075$. Inset of (a) shows the variation in the magnitude of R_T with increasing La^{3+} doping content (x) at room temperature.

To further explore the temperature dependence of total resistance (R_T) in the prepared $Ba_{1-x}La_xTiO_3$ (x = 0.0, 0.0025, 0.005, 0.0075) samples, we have plotted the total resistance (R_T = R_{Gs} + R_{GBs}) of all prepared samples measured from the Z$^{\prime}$ vs. Z$^{\prime\prime}$ plots as a function of temperature (T) in Fig. 6(a–d). Generally, the pure $BaTiO_3$ sample exhibits insulating behavior rather than semiconducting behavior, when sintered in air. Here, contrary to the common understanding regarding pure $BaTiO_3$: an insulator and ferroelectric at room temperature, the doping of La^{3+} ions in $Ba_{1-x}La_xTiO_3$ samples sintered in air at 1200 °C results in a decline in the overall resistance with a weak positive temperature coefficient of resistance (PTCR) effect. Similar results are also reported in some of the donor doped $BaTiO_3$ samples sintered at >1200 °C in air.[9,13,45] Since, in most of the PTCR ceramics, the GBs has higher electrical resistivity than the Gs interior. Thus, the ceramics with larger Gs size (i.e., less GBs density) should exhibit lower resistance value. However, the inset of Fig. 6(a) reveals that, at room temperature, the value of R_T initially decreases with the La^{3+} doping content (x) in $BaTiO_3$, reaching a minimum at x = 0.005, and then begins to increase, despite the smaller grain size. Therefore, the observed variation in R_T with La^{3+} doping content (x) in $Ba_{1-x}La_xTiO_3$ samples can be explained by the chemical defect compensation mechanism. Typically, there are two types of compensation mechanisms possible in the donor doped $BaTiO_3$ when La^{3+} ions replace Ba^{2+} ions at the A-sites of ABO_3 type perovskite crystal and are given by the following defect reactions:[16]

(i) Electronic compensation mechanism : $Ba_{Ba}{}^x \rightarrow La'_{Ba} + e'$

$$(4)$$

(ii) Ionic compensation mechanism : $4Ba_{Ba}{}^x + Ti_{Ti}{}^x \rightarrow 4La'_{Ba} + V''''_{Ti}$

$$(5)$$

At low La^{3+} doping content (x), free electrons are usually released due to the incorporation of La^{3+} ions at the Ba^{2+} site as presented in eqn (4). These free electrons are loosely bonded and can be thermally triggered to jump from the donor level to the conduction band in a semiconductor. This results in an increase in the concentration of charge carriers and a reduction in resistance. However, the minimum resistance is observed for La^{3+} doping content of x = 0.005, which is attributed to a change in the doping mechanism, i.e., a transformation from electronic compensation to ionic (cation vacancies) compensation. Thus, with the further increase in La^{3+} doping content, cation vacancies may be produced for the defect reactions as presented in eqn (5), which results in the occurrence of electronic holes. This leads to a decrease in the electronic charger carrier's concentration and an increase in resistance for x > 0.005. Moreover, one can also see from the figure that the value of R_T decreases as the temperature increases, indicating the existence of thermally stimulated conduction mechanism and confirming the semiconducting nature. However, a discontinuity is observed above the Curie temperature (T > T_c) where we observed an increasing trend of R_T with increasing temperature

in the La^{3+} doped samples. This behavior indicates a weak positive temperature coefficient of resistance (PTCR) effect in the doped samples, which is typically a GBs phenomena in the donor-doped $BaTiO_3$ samples.[46] Here, the observed PTCR effect is attributed to the fact that, above the Curie temperature (T_c), $BaTiO_3$ transforms from the ferroelectric phase (where spontaneous polarization occurs near GBs) to the paraelectric phase (where spontaneous polarization disappears) resulting in an increase in resistance due to the potential barrier increasing because of the lack of compensation for polarization induced charge.

3.5. AC conductivity

Fig. 7 depicts the temperature-dependent ac conductivity (σ_{ac}) behavior of the prepared $Ba_{1-x}La_xTiO_3$ (x = 0.0, 0.0025, 0.005, 0.0075) samples at different frequencies (1–100 kHz). As seen from the figure, the prepared samples exhibit semiconducting behavior because the value of σ_{ac} initially increases with the increase in temperature up to the Curie temperature (T_c). While, above the Curie temperature (T > T_c), the σ_{ac} value begins to decrease sharply with temperature due to their insulating behavior, as discussed earlier. Moreover, we observed that these plots can be distinguished into three different regions: two regions (R-I and R-II) at T < T_c and one region (R-III) at T > T_c, characterized by dissimilar slopes indicating distinct conduction processes with different activation energies (E_a) values. The notable change in the slopes of the prepared samples is observed between the regions R-I and R-II for T < T_c which is likely due to a difference in the rearrangement of the lattice during the transition of ferroelectric-paraelectric crystalline phase.[47] This verifies the diffuse nature of the transition along with the dominance of GBs observed earlier in Fig. 4 for the prepared samples. However, a straight line is observed in the region R-III at T > T_c revealing a sharp decrease in σ_{ac}. The activation energies (E_a) were calculated from the slopes of the linear regions of plots between ln σ and 1000/T of all prepared samples in different regions using the Arrhenius law given below:

$$\sigma = \sigma_o \exp\left(\frac{E_a}{k_B T}\right) \qquad (6)$$

where σ_o is the pre-exponential factor, E_a is the activation energy, k_B is the Boltzmann constant and T is the absolute temperature.[48] Table 2 shows the calculated values of E_a's for the prepared samples in different regions at a representative frequencies of 1 kHz, 10 kHz and 100 kHz. We found that the $BaTiO_3$ sample has a large values of E_a due to bigger grain size. While, for La^{3+} doped samples, a significant decrease in the values of E_a is observed as a result of reduced grain sizes in comparison to pure sample. Here the values of E_a are observed to increase with temperature, which shows that the conduction mechanism is a thermally activated process. While, in all doped samples, the values of E_a for R-II are bit higher than that for other regions, indicating that the GBs have a dominant effect in the total conduction of samples. Further, the values of E_a for all regions are found to decrease sharply with La^{3+} doping content
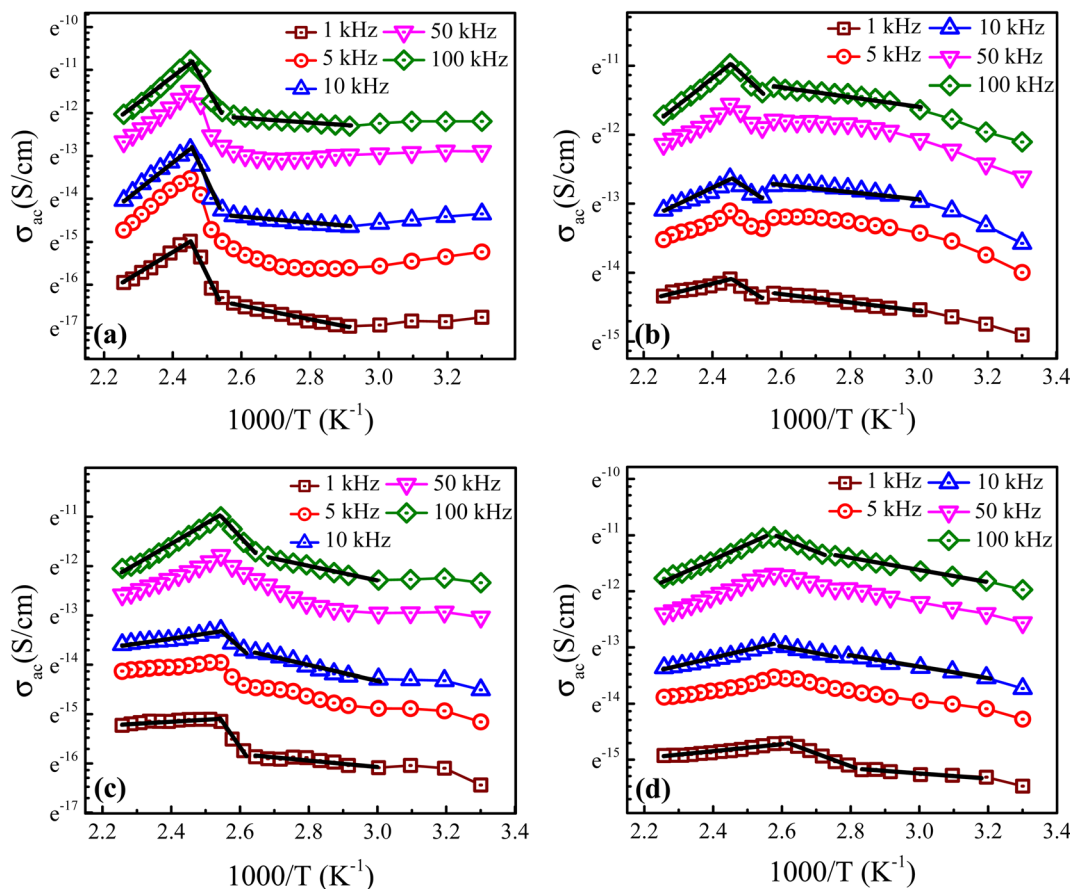
Fig. 7 Temperature-dependent ac conductivity (σ_{ac}) behavior of the prepared $Ba_{1-x}La_xTiO_3$ ceramics with (a) $x = 0.0$, (b) $x = 0.0025$, (c) $x = 0.005$, and (d) $x = 0.0075$ at different frequencies (1 kHz–100 kHz). Solid lines show the fit to the experimental data using eqn (6) at different frequency regions.

Table 2 Calculated values of activation energies (E_a's) for the prepared La^{3+} doped $Ba_{1-x}La_xTiO_3$ ceramics in different regions at a representative frequencies of 1 kHz, 10 kHz and 100 kHz

Samples (x)	Frequency (kHz)	Region-I E_a (eV)	Region-II E_a (eV)	Region-III E_a (eV)
0.0	1	0.195	1.035	0.306
	10	0.185	1.072	0.356
	100	0.166	0.902	0.381
0.0025	1	0.039	0.168	0.065
	10	0.024	0.169	0.125
	100	0.031	0.269	0.199
0.005	1	0.012	0.224	0.009
	10	0.046	0.145	0.016
	100	0.057	0.194	0.114
0.0075	1	0.008	0.032	0.013
	10	0.022	0.024	0.029
	100	0.026	0.057	0.058

(x) suggesting better conductivity of semiconducting Gs and the appearance of less conductive GBs with increasing La^{3+} doping content in the prepared $Ba_{1-x}La_xTiO_3$ ceramics.

3.6. Ferroelectric analysis

Fig. 8(a–d) shows the ferroelectric polarization *versus* electric field (P–E) hysteresis loops of $Ba_{1-x}La_xTiO_3$ ($x = 0.0, 0.0025, 0.005, 0.0075$) samples, which were measured by applying an electric field of ±10 kV cm^{-1} at room temperature. Here, the development of hysteresis loops confirms the ferroelectric nature of La^{3+} doped $BaTiO_3$ samples. With increasing La^{3+} doping content, the hysteresis loops become slimmer, which might be attributed to the donor doping and the presence of pinned polar nanoregions along with a low dielectric loss.[49,50] Moreover, it is observed that there is a slight increase in the maximum polarization (P_m) value along with a decrease in the values of remnant polarization (P_r) and coercive field (E_c) with increasing La^{3+} doping content up to $x = 0.0025$ compared to a pure $x = 0.0$ sample. With a further increase in the La^{3+} doping content ($x > 0.0025$), the value of P_m begins to decrease and becomes more or less similar to the value for pure sample. While, the values of remnant polarization (P_r) and coercive field (E_c) further decrease with increasing La^{3+} doping content and become unchanged for $x \geq 0.005$. These variations in the ferroelectric parameters could be understood in terms of the competing effects of the domain wall motion ability and the overall change in the crystal structure of $BaTiO_3$ on La^{3+}
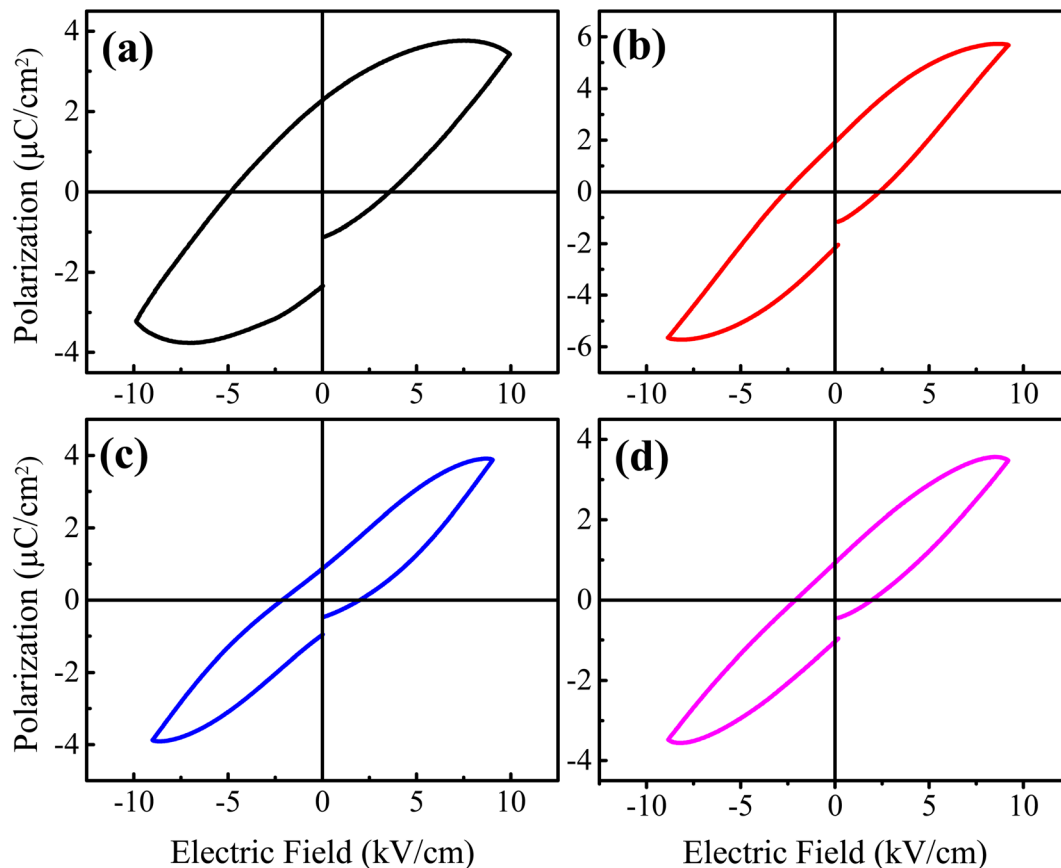
Fig. 8 Ferroelectric hysteresis loops of the prepared $Ba_{1-x}La_xTiO_3$ ceramics with (a) $x = 0.0$, (b) $x = 0.0025$, (c) $x = 0.005$, and (d) $x = 0.0075$ measured at room temperature.

doping.[26] However, for $x \geq 0.005$ samples, the relatively unchanged ferroelectric parameters suggest a critical point of La^{3+} doping content in which $BaTiO_3$ maintain the initial value of P_m along with reduced values of P_r and E_c which may be responsible for the enhancement in the energy storage density in these samples. The ferroelectric hysteresis loops were further utilized to estimate the discharge (J_d) and charge (J_c) energy storage densities of the prepared samples using the following formulas:[51]

$$J_D = \int_0^{P_m} EdP \quad (7)$$

$$J_c = \int_{P_r}^{P_m} EdP \quad (8)$$

where E and P are the applied electric field and polarization, respectively. Table 3 presents the calculated values of J_D and J_c for the prepared samples. With increasing La^{3+} doping concentration, it is found that J_D and J_c values initially increase until $x = 0.0025$, after which they begin to decrease. However, the maximum values of J_D for La^{3+} doped samples are found to be 2–3 times higher than that of pure $x = 0.0$ sample, which is accredited to the reduced grain size and remnant polarization by La^{3+} doping. Moreover, the energy storage efficiency (η) of the prepared samples was also calculated using the formula: $\eta = J_D/J_c$.[51] The calculated values of η are presented in Table 3, where a significant improvement in the energy storage efficiency is observed for La^{3+} doped $BaTiO_3$ samples in comparison to the reported values.[20,21] Here, the observed increase in the η values

Table 3 Saturation polarization (P_m), remnant polarization (P_r), coercive field (H_c), difference between the saturation and remnant polarization ($P_m - P_r$), discharge energy density (J_d), charge energy density (J_c), and energy storage efficiency (η) of the La^{3+} doped $Ba_{1-x}La_xTiO_3$ ceramics

Sample (x)	P_m ($\mu C\ cm^{-2}$)	P_r ($\mu C\ cm^{-2}$)	H_c ($kV\ cm^{-1}$)	$P_m - P_r$ ($\mu C\ cm^{-2}$)	J_d ($J\ cm^{-3}$)	J_c ($J\ cm^{-3}$)	η (%)
0.00	3.44	2.29	4.88	1.14	0.011	0.034	34
0.0025	5.66	1.87	2.63	3.79	0.035	0.052	66
0.005	3.90	0.83	2.19	3.06	0.027	0.035	78
0.0075	3.48	0.90	2.08	2.57	0.023	0.031	74

is accredited to the decrease in the slope of the hysteresis loop, the large difference in the values of P_m and P_r, high dielectric permittivity, low dielectric tangent loss, and reduced grain size. Among the prepared samples, the sample with $x = 0.005$ shows the highest energy storage efficiency of 78% at $\sim$10 kV cm^{-1}, which is found to be 2.3 times higher than that of $x = 0.0$ sample. So, the improved energy storage properties and high dielectric value of this composition make it attractive for energy storage applications.

4. Conclusions

La^{3+} doped Ba$_{1-x}$La$_x$TiO$_3$ ($x = 0.0$, 0.0025, 0.005, 0.0075) were successfully prepared by the composite-hydroxide-mediated method and their structural, dielectric, and ferroelectric properties were investigated using different analytical techniques. Rietveld refinement on the XRD patterns confirmed the formation of pure perovskite structure, while a systematic decrease in the tetragonality ratio (c/a) indicated a transformation from the tetragonal phase to a pseudo-cubic phase with La^{3+} doping content. SEM analysis showed that the La^{3+} doping inhibited the grain growth. The dielectric and impedance analysis revealed that the La^{3+} doped samples exhibit: (i) increase in the dielectric permittivity; (ii) ferroelectric–paraelectric transition around the Curie temperature; (iii) decrease in T_c towards the lower temperatures; (iv) increase in the dielectric diffusivity; and (v) the semiconducting behavior with PTCR behavior. These observed behaviors are explained in terms of a decrease in the grain size and charge compensation mechanism. While the PTCR effect results from both Gs and GBs effects, but the GBs contribution is more dominant. The P–E loops confirmed the ferroelectric behavior with a decrease in the remnant polarization and coercive field due to La^{3+} doping. Moreover, the doped samples exhibited an improvement in energy storage density and energy storage efficiency compared to that of pure undoped sample. Such a significant improvement in energy storage properties could be attributed to the reduced grain size due to La^{3+} doping. In conclusion, we found that the proposed composite-hydroxide-mediated method allowed us to fabricate dense and homogeneous microstructures with a submicron grain size ($\sim$1 μm). Among the prepared ceramics, the sample with $x = 0.005$ exhibits significantly enhanced dielectric permittivity (4381), low dielectric tangent loss (0.02), and the highest energy storage efficiency (78%) at room temperature, which makes this composition interesting for energy storage applications.

Author contributions

U. Younas: investigation, visualization, writing—original draft. M. Atif: conceptualization, supervision, writing—review & editing. A. Anjum: investigation, formal analysis. M. Nadeem: methodology, validation. T. Ali: resources, formal analysis. R. Shaheen: resources, formal analysis. W. Khalid: software, validation. Z. Ali: writing—review & editing.

Conflicts of interest

There are no conflicts to declare.

References

1 W. H. Lee and C. Y. Su, Improvement in the temperature stability of a BaTiO$_3$-based multilayer ceramic capacitor by constrained sintering, *J. Am. Ceram. Soc.*, 2007, **90**, 3345–3348.

2 C. H. Kim, K. J. Park, Y. J. Yoon, M. H. Hong, J. O. Hong and K. H. Hur, Role of yttrium and magnesium in the formation of core-shell structure of BaTiO$_3$ grains in MLCC, *J. Eur. Ceram. Soc.*, 2008, **28**, 1213–1219.

3 Z. Yang, F. Gao, H. Dua, L. Jin, L. Yan, Q. Hu, Y. Yu, S. Qu, X. Wei, Z. Xu and Y.-J. Wang, Grain size engineered lead-free ceramics with both large energy storage density and ultrahigh mechanical properties, *Nano Energy*, 2019, **58**, 768–777.

4 M. M. Vijatovic, History and Challenges of Barium Titanate Part II, *J. Sci. Sinter.*, 2008, **40**, 235–244.

5 A. Rached, M. A. Wederni, A. Belkahla, J. Dhahri, K. Khirouni, S. Alaya and R. J. Martín-Palma, Effect of doping in the physico-chemical properties of BaTiO$_3$ ceramics, *Physica B*, 2020, **596**, 412343.

6 D. Y. Lu, S. Z. Cui, Q. L. Liu and X. Y. Sun, Dielectric properties and defect chemistry of barium titanate ceramics co-doped R and Dy ions (R = Eu, Gd, Tb), *Ceram. Int.*, 2016, **42**, 14364–14373.

7 C. L. Freeman, J. A. Dawson, H.-Ru. Chen, L. Ben, J. H. Harding, F. D. Morrison, D. C. Sinclair and A. R. West, Energetics of Donor-Doping, Metal Vacancies, and Oxygen-Loss in A-Site Rare Earth-Doped BaTiO$_3$, *Adv. Funct. Mater.*, 2013, **23**, 3925–3928.

8 Y. Tsur, T. D. Dunbar and C. A. Randall, Crystal and Defect Chemistry of Rare Earth Cations in BaTiO$_3$, *J. Electroceram.*, 2001, **7**, 25–34.

9 F. D. Morrison, A. M. Coats, D. C. Sinclair and A. R. West, Charge Compensation Mechanisms in La-Doped BaTiO$_3$, *J. Electroceram.*, 2001, **6**, 219–232.

10 C. L. Freeman, J. A. Dawson, H.-R. Chen, J. H. Harding, L.-B. Ben and D. C. Sinclair, A new potential model for barium titanate and its implications for rare-earth doping, *J. Mater. Chem.*, 2011, **21**, 4861–4868.

11 S. Chatterjee, B. D. Stojanovic and H. S. Maiti, Effect of additives and powder preparation techniques on PTCR properties of barium titanate, *Mater. Chem. Phys.*, 2003, **28**, 702–710.

12 Y. L. Chen and S. F. Yang, PTCR effect in donor doped barium titanate: review of compositions, microstructures, processing and properties, *Adv. Appl. Ceram.*, 2011, **110**(5), 257–269.

13 A. Ianculescu, Z. V. Mocanu, L. P. Curecheriu, L. Mitoseriu, L. Padurariu and R. Trușcă, Dielectric and tunability properties of La-doped BaTiO$_3$ ceramics, *J. Alloys Compd.*, 2011, **509**, 10040–10049.

14 D.-Y. Lu and S.-Z. Cui, Defects characterization of Dy-doped BaTiO$_3$ ceramics via electron paramagnetic resonance, *J. Eur. Ceram. Soc.*, 2014, **34**, 2217–2227.

15 D. Makovec, N. Ule and M. Drofenik, Positive Temperature Coefficient of Resistivity Effect in Highly Donor-Doped Barium Titanate, *J. Am. Ceram. Soc.*, 2001, **84**, 1273–1280.

16 M. M. Vijatović Petrović, J. D. Bobić, R. Grigalaitis, B. D. Stojanović and J. Banys, La-doped and La/Mn-co-doped Barium Titanate Ceramics, *Acta Phys. Pol., A*, 2013, **124**, 155–160.

17 F. D. Morrison, D. C. Sinclair and A. R. West, An Alternative Explanation for the Origin of the Resistivity Anomaly in La-Doped BaTiO$_3$, *J. Am. Ceram. Soc.*, 2001, **84**(2), 474–476.

18 M. Ganguly, S. K. Rout, T. P. Sinha, S. K. Sharma, H. Y. Park, C. W. Ahn and I. W. Kim, Characterization and Rietveld Refinement of A-site deficient Lanthanum doped Barium Titanate, *J. Alloys Compd.*, 2013, **579**, 473–484.

19 Y. Wang, K. Miao, W. Wang and Y. Qin, Fabrication of lanthanum doped BaTiO$_3$ fine-grained ceramics with a high dielectric constant and temperature-stable dielectric properties using hydro-phase method at atmospheric pressure, *J. Eur. Ceram. Soc.*, 2017, **37**, 2385–2390.

20 V. S. Puli, P. Li, S. Adireddy and D. B. Chrisey, Crystal structure, dielectric, ferroelectric and energy storage properties of La-doped BaTiO3 semiconducting ceramics, *J. Adv. Dielectr.*, 2015, **5**, 1550027.

21 R. Kumar, I. Singh, R. Meena, K. Asokan, B. Birajdar and S. Patnaik, Effect of La-doping on dielectric properties and energy storage density of lead-free Ba(Ti$_{0.95}$Sn$_{0.05}$)O$_3$ ceramics, *Mater. Res. Bull.*, 2020, **123**, 110694.

22 T. Badapanda, V. Senthil, S. Panigrahi and S. Anwar, Diffuse phase transition behavior of dysprosium doped barium titanate ceramic, *J. Electroceram.*, 2013, **31**, 55–60.

23 H.-J. Chen and Y.-W. Chen, Hydrothermal Synthesis of Barium Titanate, *Ind. Eng. Chem. Res.*, 2003, **42**(3), 473–483.

24 R. Ashiri, A. Nemati, M. S. Ghamsari, S. Sanjabi and M. Aalipour, A modified method for barium titanate nanoparticles synthesis, Mater, *Res. Bull.*, 2011, **46**, 2291–2295.

25 D. Chen and X. Jiao, Solvothermal Synthesis and Characterization of Barium Titanate Powders, *J. Am. Ceram. Soc.*, 2000, **83**, 2637–2639.

26 S. Sharma, R. K. Patel, C. Prakash and P. Kumar, Structural, dielectric and ferroelectric study of microwave sintered lanthanum substituted BaTiO$_3$ ceramics, *Mater. Chem. Phys.*, 2011, **130**, 191–195.

27 M. Borah and D. Mohanta, Composite-Hydroxide-Mediated Formation of Barium Titanate Nanocubes and Their Optical Emission Response, *Chin. J. Phys.*, 2015, **53**, 020804.

28 T. M. Khan, M. Zakria, R. I. Shakoor and S. Hussain, Composite-hydroxide-mediated approach an effective synthesis route for BaTiO$_3$ functional nanomaterials, *Appl. Phys. A*, 2016, **122**, 274.

29 Y. Xie, S. Yin, T. Hashimoto, Y. Tokano, A. Sasaki and T. Sato, Low temperature synthesis of tetragonal BaTiO$_3$ by a novel composite-hydroxide-mediated approach and its dielectric properties, *J. Eur. Ceram. Soc.*, 2010, **30**, 699–704.

30 Joint Committee on Powder Diffraction Standards, Powder Diffraction Files no. 05-0626.

31 A. E. Ghandouri, S. Sayouri, T. Lamcharfi and A. Elbasset, Structural, microstructural and dielectric properties of Ba$_{1−x}$La$_x$Ti$_{(1−x/4)}$O$_3$ prepared by sol gel method, *J. Adv. Dielectr.*, 2019, **9**, 1950026.

32 R. D. Shannon, Revised effective ionic radii in halides and chalcogenides, *Acta Crystallogr., Sect. A: Found. Crystallogr.*, 1976, **32**, 751–767.

33 X. Liu, R. Hong and C. Tian, Tolerance factor and the stability discussion of ABO3-type ilmenite, *J. Mater. Sci.: Mater. Electron.*, 2009, **20**, 323–327.

34 Z. Lv, J. Wei, T. Yang, Z. Sun and Z. Xu, Manipulation of Curie temperature and ferroelectric polarization for large electrocaloric strength in BaTiO$_3$-based ceramics, *Ceram. Int.*, 2020, **46**, 14978–14984.

35 L. Pdungsap, N. Udomkan, S. Boonyuen and P. Winotai, Optimized conditions for fabrication of La-dopant in PZT ceramics, *Sens. Actuators, A*, 2005, **122**, 250–256.

36 S. M. Bobade, D. D. Gulwade, A. R. Kulkarni and P. Gopalan, Dielectric properties of A- and B-site-doped BaTiO$_3$ (I): La- and Al-doped solid solutions, *J. Appl. Phys.*, 2005, **97**, 074105.

37 Y. Tan, J. Zhang, Y. Wu, C. Wang, V. Koval, B. Shi, H. Ye, R. McKinnon, G. Viola and H. Yan, Unfolding grain size effects in barium titanate ferroelectric ceramics, *Sci. Rep.*, 2015, **5**, 9953.

38 Z. Raddaoui, S. El Kossi, J. Dhahri, N. Abdelmoula and K. Taibi, Study of diffuse phase transition and relaxor ferroelectric behavior of Ba$_{0.97}$Bi$_{0.02}$Ti$_{0.9}$Zr$_{0.05}$Nb$_{0.04}$O$_3$ ceramic, *RSC Adv.*, 2019, **9**, 2412–2425.

39 K. Uchino and S. Nomura, Critical exponents of the dielectric constants in diffused-phase-transition crystals, *Ferroelectrics*, 1982, **44**, 55–61.

40 X.-G. Tang and H. L.-W. Chan, Effect of grain size on the electrical properties of (Ba,Ca)(Zr,Ti)O3 relaxor ferroelectric ceramics, *J. Appl. Phys.*, 2005, **97**(3), 034109.

41 Y. Wang, Y. Pu, X. Li and H. Zheng, Structural evolution, relaxation behaviors and dielectric properties of BaTiO$_3$–BiAlO$_3$ perovskite solid solutions, *J. Mater. Sci.: Mater. Electron.*, 2016, **27**, 11565–11571.

42 E. Barsoukov and J. R. Macdonald, *Impedance Spectroscopy Theory, Experiments and Applications*, Wiley, New York, 2005.

43 M. Younas, M. Nadeem, M. Atif and R. Grossinger, Metal-semiconductor transition in NiFe$_2$O$_4$ nanoparticles due to reverse cationic distribution by impedance spectroscopy, *J. Appl. Phys.*, 2011, **109**, 093704.

44 J. T. S. Irvine, D. C. Sinclair and A. R. West, Electroceramics: Characterization by Impedance Spectroscopy, *Adv. Mater.*, 1990, **2**, 132.

45 K. Matsuura, T. Hoshina, H. Takeda, Y. Sakabe and T. Tsurumi, Effects of Ca substitution on room temperature resistivity of donor-doped barium titanate based PTCR ceramics, *J. Ceram. Soc. Jpn.*, 2014, **122**(6), 402–405.

46 J. Nowotny and M. Rekas, Positive Temperature Coefficient of Resistivity for BaTiO$_3$-based Materials, *Ceram. Int.*, 1991, **17**, 227.

47 S. Ben Moumen, A. Neqali, B. Asbani, D. Mezzane, M. Amjoud, E. Choukri, Y. Gagou, M. El Marssi and I. Lukyanchuk, Impedance spectroscopy studies on lead free $Ba_{1-x}Mg_x(Ti_{0.9}Zr_{0.1})O_3$ ceramics, *Superlattices Microstruct.*, 2018, **118**, 45–54.

48 A. U. Rehman, M. Atif, M. Younas, T. Rafique, H. Wahab, A. Ul-Hamid, N. Iqbal, Z. Ali, W. Khalid and M. Nadeem, Unusual semiconductor–metal–semiconductor transitions in magnetite Fe_3O_4 nanoparticles, *RSC Adv.*, 2022, **12**, 12344.

49 Y. H. Huang, Y. J. Wu, W. J. Qiu, J. Li and X. M. Chen, Enhanced energy storage density of Ba0.4Sr0.6TiO3–MgO composite prepared by spark plasma sintering, *J. Eur. Ceram. Soc.*, 2015, **35**, 1469–1476.

50 W. Kleemann, The relaxor enigma–charge disorder and random fields in ferroelectrics, *J. Mater. Sci.*, 2006, **41**, 129–136.

51 Y. Lin, D. Li, M. Zhang, S. Zhan, Y. Yang, H. Yang and Q. Yuan, Excellent Energy-Storage Properties Achieved in BaTiO$_3$-Based Lead-Free Relaxor Ferroelectric Ceramics via Domain Engineering on the Nanoscale, *ACS Appl. Mater. Interfaces*, 2019, **11**, 36824–36830.